PNAS RESEARCH ARTICLE | PLANT BIOLOGY

Modeling reveals posttranscriptional regulation of GA metabolism enzymes in response to drought and cold

Leah R. Band[a,b,1], Hilde Nelissen[c,d], Simon P. Preston[b], Bart Rymen[e], Els Prinsen[f], Hamada AbdElgawad[f,g], and Gerrit T. S. Beemster[f]

Edited by Mark Estelle, University of California at San Diego, La Jolla, CA; received December 8, 2021; accepted May 27, 2022

The hormone gibberellin (GA) controls plant growth and regulates growth responses to environmental stress. In monocotyledonous leaves, GA controls growth by regulating division–zone size. We used a systems approach to investigate the establishment of the GA distribution in the maize leaf growth zone to understand how drought and cold alter leaf growth. By developing and parameterizing a multiscale computational model that includes cell movement, growth-induced dilution, and metabolic activities, we revealed that the GA distribution is predominantly determined by variations in GA metabolism. Considering wild-type and UBI::GA20-OX-1 leaves, the model predicted the peak in GA concentration, which has been shown to determine division–zone size. Drought and cold modified enzyme transcript levels, although the model revealed that this did not explain the observed GA distributions. Instead, the model predicted that GA distributions are also mediated by posttranscriptional modifications increasing the activity of GA 20-oxidase in drought and of GA 2-oxidase in cold, which we confirmed by enzyme activity measurements. This work provides a mechanistic understanding of the role of GA metabolism in plant growth regulation.

gibberellin | environmental conditions | plant hormones | maize leaf growth | mathematical modeling

Significance

Understanding why plant growth decreases in drought and cold is essential to ascertaining how these conditions affect crop yields. Previous studies have shown that growth depends on the distribution of the hormone gibberellin (GA). By developing a computational model and comparing predictions with GA measurements, we show that the GA distribution is mainly created by spatial variations in GA synthesis and degradation. We reveal that although the synthesis and degradation enzyme transcripts are affected by drought and cold, this does not explain the GA distributions. Instead, we find that specific enzyme activities are increased to create the GA distributions that underlie the growth responses. Thus, we gain an understanding of plant growth inhibition by drought and cold.

The hormone gibberellin (GA) controls plant growth and plays a key role in growth responses to environmental conditions (1, 2). This growth regulation is thought to be underpinned by the GA distribution; however, how the GA distribution is regulated is largely unknown. In roots and monocotyledonous leaves, the sizes of the division zone (DZ) and elongation zone (EZ) are key parameters that determine overall organ growth rates (3–6). The boundaries of these growth zones are dynamically controlled by hormone distributions (7), which depend on hormone metabolism, transport between cells, and dilution (due to cell growth). In *Arabidopsis* roots, for example, the DZ size has been shown to be regulated by GA synthesis (8–10), GA signaling (11), auxin transport (12, 13), and cross talk between auxin and cytokinin (14–16).

Maize leaves provide an alternative organ for studying growth regulation, with the major advantage that they enable the direct measurement of spatial distributions of hormone and transcript levels and enzyme activities along the growth zone (9, 17). In maize leaves, bioactive gibberellins, GA_1 and GA_4, show a distinct maximum within the DZ (9, 17). Kinematic and hormone analysis of wild-type leaves, *dwarf3* leaves (defective in GA synthesis), and UBI::GA20-OX-1 leaves (overexpressing a key GA 20-oxidase (GA20ox) biosynthesis enzyme) has demonstrated that the GA_1 distribution determines the length of the DZ (9) (similar to its function in the *Arabidopsis* root [8], although sensor observations suggest GA distribution differs [18]). Thus, the expression of GA metabolic enzymes plays a key role in creating GA_1 distribution and controlling DZ size (9). These GA metabolic enzymes also mediate growth responses to cold (19, 20), salt (21), nutrients (10, 22), light (23), and water (24) and cross talk between the growth-regulatory hormone pathways (25, 26), making them a key component of environmental growth responses.

Although metabolite and transcript measurements along the growth zone provide insights into how hormone levels are related to local cell division and expansion, they essentially produce static measurements, making it hard to infer the underlying dynamic processes. Understanding how molecular and cellular processes interact to establish, maintain, and adjust the hormone distributions that control organ growth can be challenging, and theoretical models have proven invaluable in providing a mechanistic understanding (13, 14, 16, 27–29). Considering the GA dynamics within the *Arabidopsis* root, previous modeling demonstrated that cell elongation causes significant dilution in the EZ (28). Thus, in contrast to auxin distribution being primarily determined by carrier-mediated transport (12, 13), the GA distribution appears to be controlled by an entirely different mechanism.

In this study, we gain a mechanistic understanding of how GA distributions are controlled. We developed a multiscale model of GA dynamics within the maize leaf growth

Author contributions: L.R.B., H.N., and G.T.S.B. designed research; L.R.B., H.N., S.P.P., B.R., E.P., and H.A.E. performed research; L.R.B., H.N., S.P.P., B.R., H.A.E., and G.T.S.B. analyzed data; and L.R.B. and G.T.S.B. wrote the paper.

The authors declare no competing interest.

This article is a PNAS Direct Submission.

[1]To whom correspondence may be addressed. Email: leah.band@nottingham.ac.uk.

This article contains supporting information online at http://www.pnas.org/lookup/suppl/doi:10.1073/pnas.2121288119/-/DCSupplemental.

Published July 25, 2022.

zone by combining a detailed model of the GA metabolism within each cell with cellular growth dynamics. Focusing on the maize leaf enabled us to compare model predictions to spatial metabolite and enzyme data (which is not feasible in smaller species such as *Arabidopsis* [17]), revealing that bioactive GA distribution is predominantly determined by spatial variations in metabolism.

We applied the model to investigate how drought and cold affect GA distribution, to understand how these stresses alter leaf growth. Mild drought reduces maize leaf growth by reducing DZ size, bioactive GA levels, and the transcript levels of the GA20ox biosynthesis enzymes (30). The model revealed that GA20ox activity is increased to counteract the reduction in *GA20ox* transcripts, suggesting that the lower bioactive GA levels and growth response are mediated instead by increased transcription of the GA 2-oxidase (GA2ox) catabolic enzymes.

The role of GA in the response to cold, which inhibits cell division rates but not DZ size (31), is still unclear. Measurements revealed a substantial reduction in the *GA2ox* transcripts, suggesting that cold reduces GA degradation. However, the model showed that GA2ox activity is increased to counteract the reduced transcript levels and maintain bioactive GA concentrations at control levels. Thus, the model reveals insights into drought and cold responses, suggesting that the modulation of specific oxidation rates determines the bioactive GA distributions that underpin growth regulation.

Results

Model description. To understand how GA distribution is regulated, we constructed a cell-based model that describes GA biosynthesis, degradation, and dilution (due to cell growth) within the maize leaf growth zone (Fig. 1 *A* and *B*). The model exploits the simple linear leaf geometry and represents the leaf as a single file of cells. Based on a stable leaf elongation rate during the first 5 d after emergence (31), we considered leaf growth to be in steady state. The model integrates cell growth and division rates from experimental measurements (32) (Fig. 1 *C*–*F*). Cell length decreases slightly close to the base of the leaf before increasing with distance along the growth zone (Fig. 1*C*). Velocity is zero at the base of the leaf and increases with distance along the growth zone (Fig. 1*D*). Using these data, we calculated the relative elongation rates (Fig. 1*E*), which follow a roughly bell-shaped curve, and the cell division rates (Fig. 1*F*), which show a bell-shaped curve spanning the DZ. The model also integrates the increase in the leaf's cross-sectional area along the growth zone to accommodate increases in cell volume when simulating dilution (33). Consistent with the approximate doubling of both the width and thickness of the leaf (33), volumetric quantifications showed that the leaf cross-section increases more than fivefold across the growth zone (Fig. 1*G*). With these growth dynamics (Fig. 1 *C*–*F*), the maize leaf growth zone is represented by a file of approximately 1,400 cells, with ∼700 cells in the DZ and ∼700 cells in the EZ. These growth dynamics are used to simulate dividing and growing cells (*SI Appendix*).

In the model, we incorporated the subcellular structure of the cells. Within the DZ, cells predominantly contain a nucleus and cytoplasm; we assumed that the nuclear volume is constant and equal to 50% of the cell volume at the most basal position (noting that the nuclear volume stays constant in the virtual absence of endoreduplication in maize leaves [31]) and thus that cell growth in the DZ occurs due to cytoplasmic expansion. Within the EZ, growth occurs primarily by rapidly increasing vacuolar volume. Based on cell length and cross-sectional area distributions (Fig. 1 *C* and *G*), we calculated that cell volume increases ∼12-fold over the EZ, which, under the assumption of vacuolar expansion (with no increase in the nucleus or cytoplasm volume), results in the volume of the cells' vacuole being approximately 92% of the cells' volume when they enter the mature zone. This value agrees with previous suggestions that the vacuole takes up 90 to 95% of the cell volume (34).

GA biosynthesis involves a series of oxidation steps, converting the precursor, geranylgeranyldiphosphate, to the bioactive GA_4 and GA_1 (35, 36). GA biosynthesis has been shown to be predominantly regulated at the later steps of this pathway (37), whereby GA_{53} and GA_{12} are converted to bioactive GAs (35, 36). Focusing on the pathway that leads to the more prevalent bioactive GA in maize, GA_1 (9) (Fig. 1*B*), we simulated GA biosynthesis and degradation within each cell: GA_{53} undergoes a series of oxidation steps mediated by GA20ox to produce GA_{20}, which is converted to the bioactive GA_1 by GA 3-oxidase (GA3ox) (35). GA2ox degrade the bioactive GA_1 and precursor GA_{20} to GA_8 and GA_{29}, respectively, which are in turn converted by the GA2ox to their catabolite forms (35). We represented these reactions by a system of ordinary differential equations (ODEs) for the metabolite, enzyme, and complex concentrations: Each step was modeled using the law of mass action by assuming the GA metabolite first binding to the enzyme with a reversible reaction, and the resulting complex then dissociating into the next GA metabolite in the pathway and the enzyme (38). We assumed that enzymes are translated at a rate proportional to the transcript level.

The reactions involved in the GA metabolism pathway downstream of GA_{53} occur in the cytoplasm (35, 36), and we assumed that the enzymes and complexes are only present in this compartment. Data in *Arabidopsis* suggest that GA metabolites are also present in the nucleus and the vacuole (39). In absence of analogous data in maize, we assumed this to be similar in maize, hence within the model assuming equal metabolite concentrations throughout the cell.

Prescribing the growth dynamics and distributions of the GA_{53} concentration and *GA20ox*, *GA3ox*, and *GA2ox* transcript levels, the cell-based model could be simulated to predict the distributions of the downstream metabolites, enzymes, and complexes. The spatial distributions of the GA_{53} concentration and *GA20ox*, *GA3ox*, and *GA2ox* transcript levels are upstream inputs, each of which were represented by a sum of b-spline functions (40) with coefficients that were estimated using the experimental data as part of the model fitting (*SI Appendix*).

To summarize, we developed a cell-based model that describes GA metabolism and dilution within the maize leaf growth zone; the key assumptions behind this cell-based model (described above) are compiled in *SI Appendix*, Table S1.

Derivation of a reduced model. The cell-based model comprises 17 ODEs for each cell in the growth zone, which for 1,400 cells results in a system of 25,200 ODEs, which can be simulated until they reach a steady state. For a given parameter set, the cell-based model took several hours to run to predict the steady-state distributions, making detailed parameter surveys impractical. To estimate model parameter values that enable the model to reproduce the experimental data, we needed to derive a reduced model to reduce the simulation time (Fig. 2*A*). We derived a continuum description of the cell-based model, considering quantities in terms of distance from the leaf base. We further reduced the model by assuming that

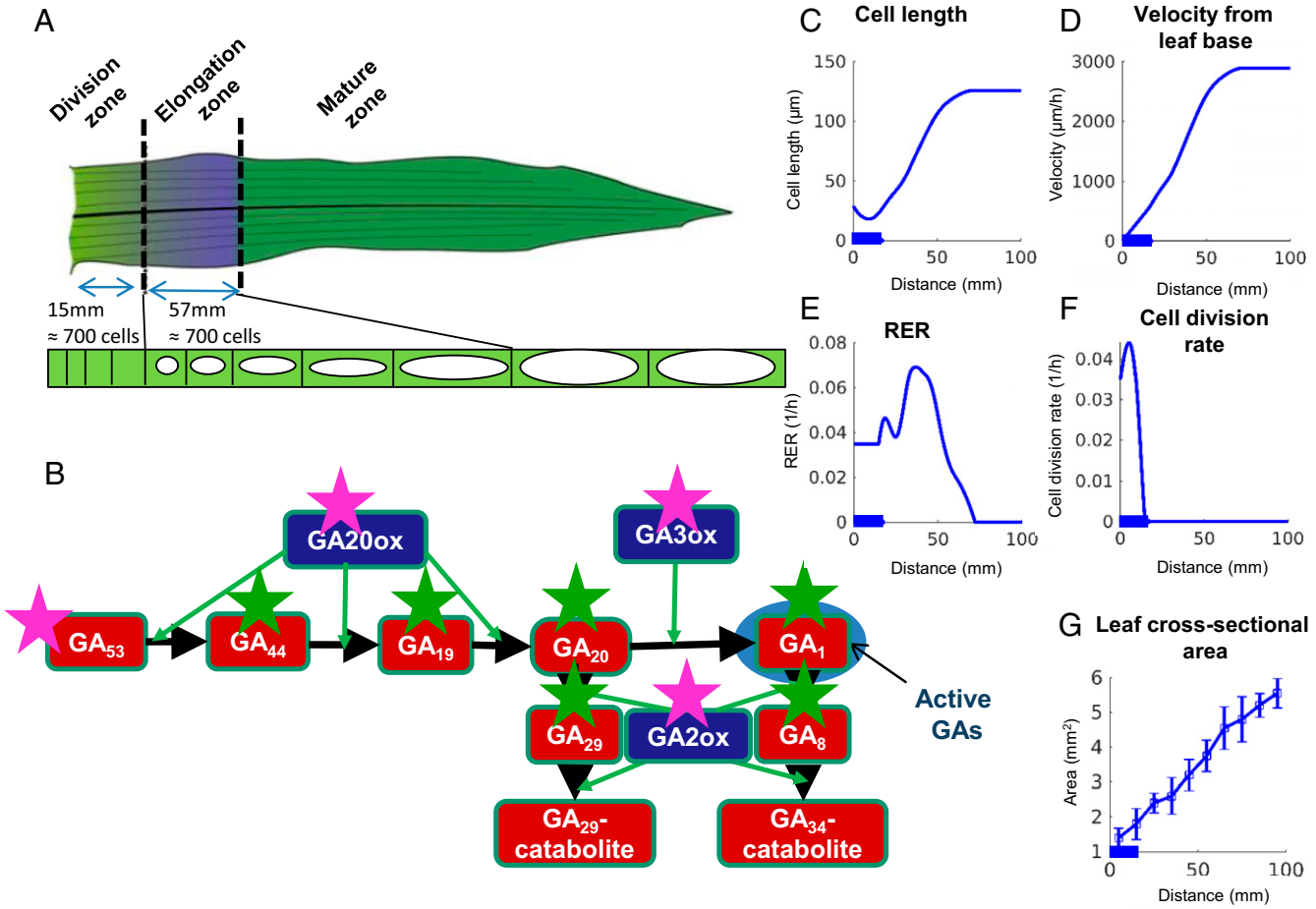

Fig. 1. Model summary. (*A*) Schematic representation of the maize leaf showing the division, elongation, and mature zones. We model the leaf as a file of cells, with cytoplasmic expansion in the division zone and vacuolar expansion in the elongation zone. (*B*) The gibberellin biosynthesis and degradation network. In the network diagram, red boxes are used for the metabolites, blue boxes are used for the enzymes, pink stars label the components modeled as input/forcing functions (parameterized via data on GA_{53} metabolite levels and gene expression levels of *GA20ox*, *GA3ox*, and *GA2ox*), and green stars label the components that are solutions of the ODEs (which are fitted to measurements of the corresponding metabolites). (*C*–*G*) Growth dynamics for maize leaf 4, B73. (*C*) Experimental measurements of cell lengths away from the leaf base; data show averages calculated via interpolation using measurements from $n = 3$ leaves. (*D*) Cell velocities calculated from data in (*C*). (*E*) Cell relative elongation rates (RERs) calculated from data in (*D*). (*F*) Cell division rates calculated from data in (*C*) and (*D*). (*G*) Experimental data for the leaf cross-sectional area (mean ± SE with $n = 10$). *C*–*F* show bars at the x-axis marking the DZ region ($n = 3$). The corresponding growth dynamics for other cases are shown in *SI Appendix*, Figs. S1–S3.

the ratio between the enzyme concentrations and metabolite concentrations are small (an approximation typically taken when modeling enzyme reactions [41] and shown previously to be appropriate for GA20ox-mediated oxidation [42]). The resulting reduced model involved a system of six ODEs in terms of distance from the leaf base for the concentrations of GA_{44}, GA_{19}, GA_{20}, GA_1, GA_{29}, and GA_8 (highlighted with green stars in Fig. 1*B*) that depend on eight oxidation rate constants (one associated with each oxidation step, which encompasses the translation rate, binding rates, and enzyme activity), the four input functions (representing the spatial distributions of GA_{53} concentration and *GA20ox*, *GA3ox*, and *GA2ox* transcript levels; pink stars in Fig. 1*B*), and the prescribed growth dynamics.

To aid clarity, we provide a summary of the model assumptions underlying the reduced model in *SI Appendix*, Table S1. As described in the text below, using the reduced model, we were able to estimate the reduced model parameters for a given experimental dataset, and therefore all model results presented in Figs. 2–5 were created by simulating the reduced model.

GA_1 distribution is predominantly determined by spatial variations in metabolism. To test whether the reduced model could represent our observations, we initially parameterized the reduced model using published experimental measurements of metabolite and transcript levels within 12 leaf segments along the maize leaf growth zone, fitting the reduced model parameters independently to data from B104 (9) and B73 inbred lines (30). Prior to fitting, we converted the metabolite measurements (in ng/gDW) (*SI Appendix*, Figs. S4 and S5) to nM concentrations (*SI Appendix*, Figs. S6 and S7). After the conversion, the spatial metabolite distribution profiles were globally similar to the original data but could differ in detail; for example, in the nM concentration profile, the peak GA_1 was slightly closer to the leaf base than in the corresponding GA_1 measurements (*SI Appendix*, Fig. S8). Based on these data, we estimated parameters by minimizing a weighted sum-of-squares criterion (detailed in *SI Appendix*, section 2.3.4). With the estimated parameters, the reduced model showed a reasonable agreement with the experimental measurements (Fig. 2 *B*–*K* and *SI Appendix*, Fig. S10) and faithfully reproduced the peak in the cytoplasmic GA_1 level within the DZ (Fig. 2*I*).

Using the reduced model enabled us to estimate the model parameters (i.e., the rate constants in the metabolism network); thus, we were able for the first time to assess the relative impact of individual cellular and subcellular processes on the established GA_1 distribution. Removing either the presence of dilution

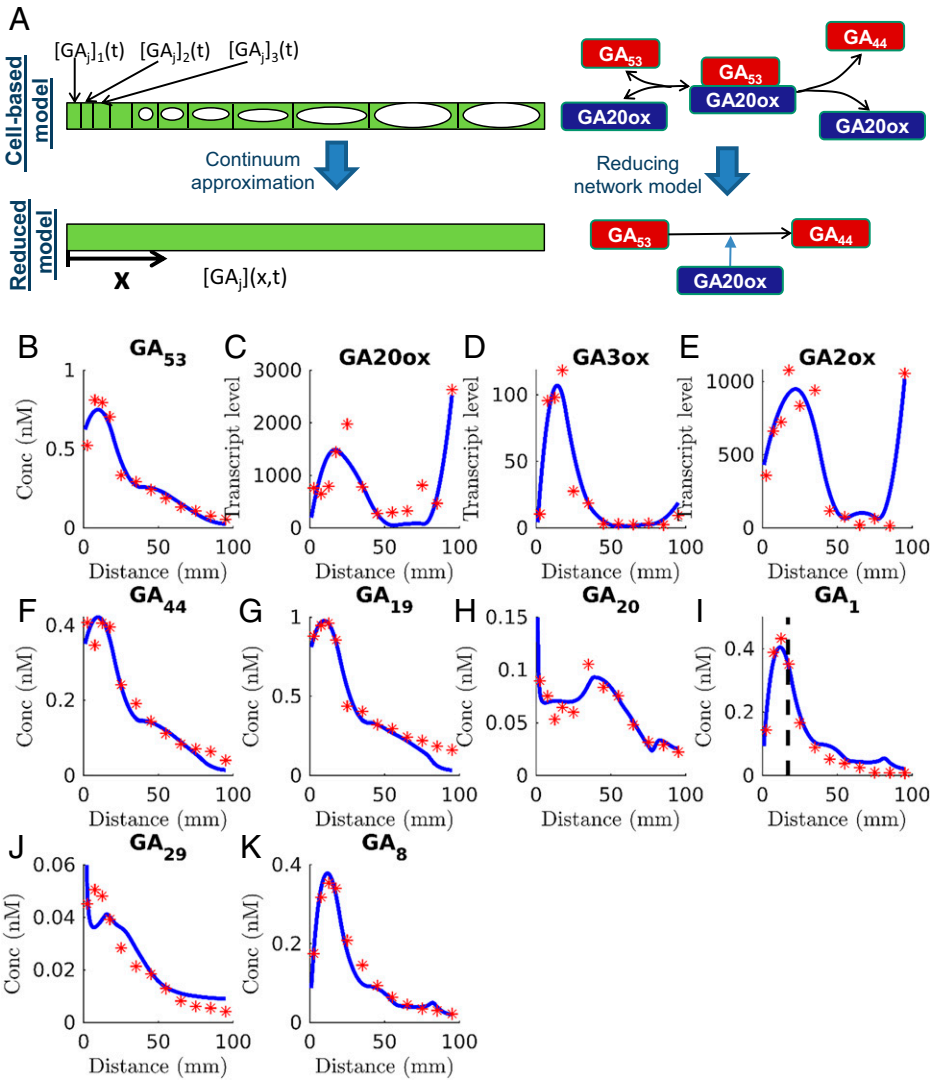

Fig. 2. Summary and predictions of the reduced model, fitted to the control wild-type data for B73. (*A*) Schematic summarizing the differences between the original cell-based model and the reduced model. (*B*–*K*) Measured and predicted distributions of GA metabolites and enzymes along the maize leaf. Data for B73 maize are shown with red stars and fitted reduced model predictions are shown with solid blue lines. (*I*) also shows the mean position of the boundary between the DZ and EZ (dashed black lines; *SI Appendix*, Table S3, $n = 3$). Metabolite data (*B*, *F*–*K*) show mean concentrations calculated from mean values from data on metabolite levels (*SI Appendix*, Fig. S4), dry weight (*SI Appendix*, Fig. S3*C*), and leaf cross-sectional area (*SI Appendix*, Fig. S3*A*). Transcript data (*C*–*E*) show mean values for $n = 3$–7 (positions 0–30 and 95 mm) and $n = 1$–3 (positions 35–85 mm).

(Fig. 3*A*) or the presence of cell movement (Fig. 3*B*), or the presence of both dilution and cell movement (Fig. 3*C*), had little effect on the predicted GA distributions. Similar results were obtained for B104 (*SI Appendix*, Fig. S10). The influence of dilution and cell movement on the GA distribution depends on the magnitudes of the rate constants—with the estimated rate constants, the metabolism network quickly reaches an equilibrium within each cell so that dilution and cell movement are slower processes that have little effect on the predicted GA concentrations (*SI Appendix*, Fig. S11, which shows how dilution and cell movement have an effect on the GA_1 distribution if the rate constants are smaller). We conclude that dilution and cell movement have only minor effects on the GA distributions and that the GA_1 distribution is predominantly determined by the spatial variations in metabolism.

The estimated parameters provide insights into the mechanisms that determine the distributions of the GA metabolites and differences between B73 and B104. The parameter estimates obtained (*SI Appendix*, Table S2) suggest that for B73 the GA2ox-mediated degradation rate of the precursor GA_{20} is small but that there is a faster GA3ox-mediated conversion of GA_{20} to the bioactive GA_1, which explains the low GA_{20} concentrations observed. In contrast, for B104, the degradation of GA_{20} is fast, whereas the conversion of GA_{20} to GA_1 is slower. To test this model prediction experimentally, we therefore directly compared the rates of GA2ox and GA3ox in the growth zone of B73 and B104 leaves. In agreement with the model prediction, these data revealed that in B73, GA3ox enzyme activity (producing GA_1) is consistently higher than GA2ox activity (producing GA_{29}; Fig. 3*D*). Moreover, as predicted by the model, in B104 the inverse situation occurs (Fig. 3*E*).

As one may expect, doubling the GA20ox-mediated oxidation rates increased the predicted GA_1 concentrations (Fig. 3*F* and *SI Appendix*, Fig. S12), whereas doubling the GA2ox rates decreased the predicted GA_1 concentrations (Fig. 3*F* and *SI Appendix*, Fig. S13), although the qualitative features of the GA_1 distribution remained the same. Varying the oxidation rate associated with the GA3ox-mediated step had little effect on the GA_1 predictions (Fig. 3*F* and *SI Appendix*, Fig. S14; doubling the GA3ox oxidation rate increased the rate at which GA_{20} is converted to GA_1, but this also decreased the

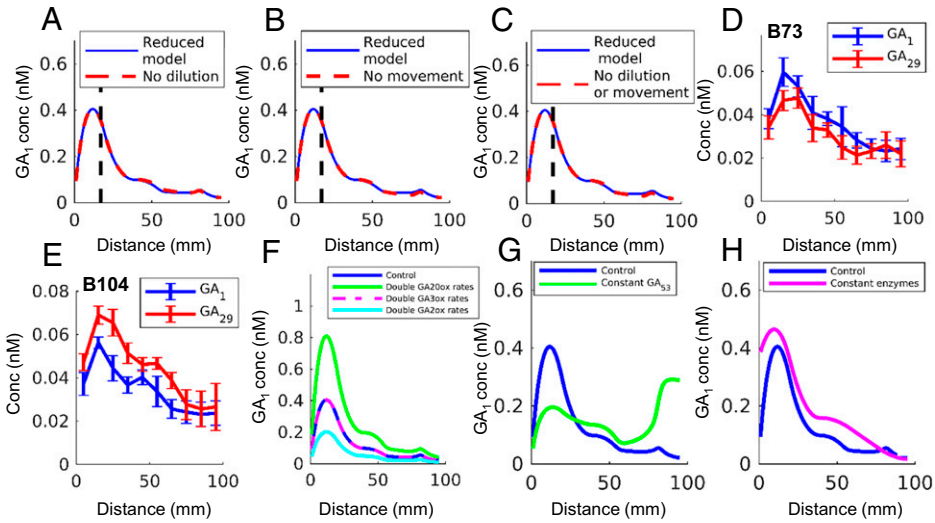

Fig. 3. Analyzing the reduced model predictions for control, wild-type dynamics. (*A–C*) Effect of model components on the predicted cytoplasmic GA_1 concentration: (*A*) with (solid line) and without (dashed red line) dilution; (*B*) with (solid line) and without (dashed red line) cell movement away from the leaf base; (*C*) with (solid line) and without (dashed red line) dilution and cell movement away from the leaf base. (*D,E*) Degradation/oxidation of GA_{20} by GA2ox (production rate of GA_{29}) and GA3ox (production rate of GA_1) in (*D*) B73 and (*E*) B104 wild-type leaves. Data show mean ± SE for $n = 4$. (*F*) Effect of the oxidation rates on the predicted GA_1 distribution. *(G)* Effect of setting the GA_{53} concentrations to be spatially constant on the predicted GA_1 distribution. (*H*) Effect of setting the enzyme transcript levels to be spatially constant on the predicted GA_1 distribution (for [*F–H*], see *SI Appendix*, Figs. S12–S16 for the corresponding predictions of the other components). (*A–C*) also show the mean position of the boundary between the DZ and EZ (dashed black lines; *SI Appendix*, Table S3, $n = 3$).

GA_{20} concentrations: at quasi-steady state these processes canceled each other out, resulting in little effect on the GA_1 distribution).

The reduced model also enabled us to investigate the importance of the spatial distributions of the GA_{53} metabolite and enzyme transcript levels. With constant GA_{53}, the predicted GA_1 formed only a small peak in the DZ and increased as cells left the growth zone (Fig. 3*G* and *SI Appendix*, Fig. S15), whereas with constant enzyme levels, the GA_1 peak in the DZ was less pronounced (Fig. 3*H* and *SI Appendix*, Fig. S16). We

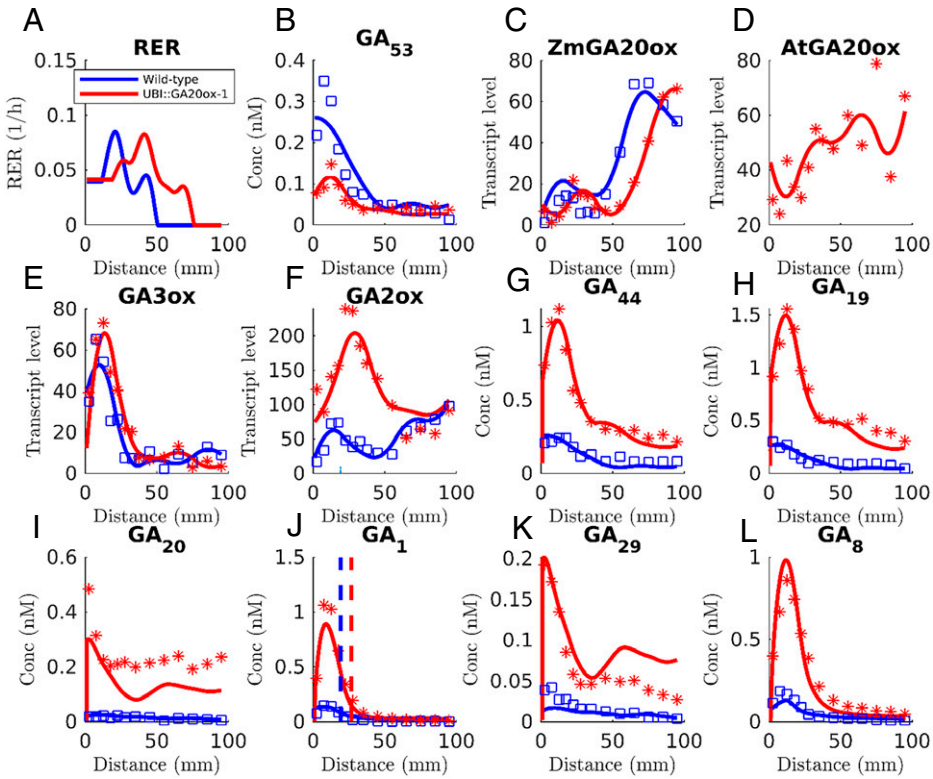

Fig. 4. Effect of GA20ox overexpressing line (UBI::GA20-OX-1) on GA pathway. (*A*) RERs for wild-type and GA20ox overexpressing line (UBI::GA20-OX-1), calculated from mean cell velocity data given in *SI Appendix*, Fig. S2 ($n = 3$). (*B–L*) Measured and predicted distributions of GA metabolites and enzymes along the maize leaf for wild-type (blue) and the GA20ox overexpressing line (UBI::GA20-OX-1) (red). Data shown with blue squares (control) and red stars (UBI::GA20-OX-1); fitted model predictions are shown with solid lines. Predictions are from the reduced model with estimated parameters given in *SI Appendix*, Table S4. Metabolite data (*B*, *G–L*) show mean concentrations calculated from mean values from data on metabolite levels (*SI Appendix*, Fig. S5), dry weight (*SI Appendix*, Fig. S3*C*), and leaf cross-sectional area (*SI Appendix*, Fig. S3*B*). Transcript data (*C–F*) show mean values for $n = 3$. (*J*) also shows the mean position of the boundary between the DZ and EZ for wild-type (dashed blue line) and UBI::GA20OX-1 (dashed red line), $n = 3$.

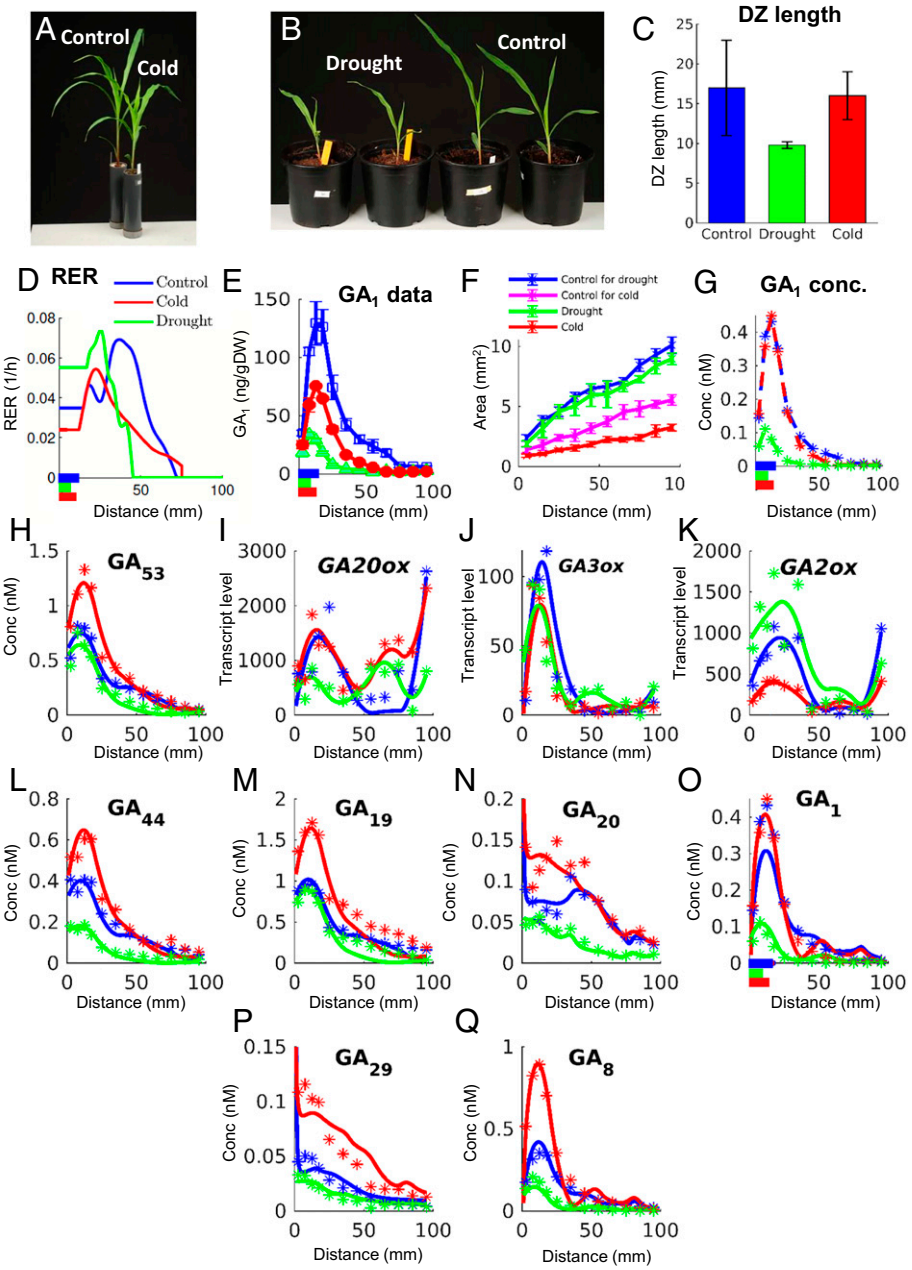

Fig. 5. Influence of drought and cold on GA pathway. (*A*) B73 maize plants subjected to cold conditions. (*B*) B73 maize plants subjected to drought conditions. (*C*) Measured DZ lengths in control (blue), drought (green), and cold (red) condition (mean ± SE with $n = 3$ replicates). (*D*) RERs in control (blue), drought (green), and cold conditions (red). (*E*) Measured bioactive GA_1 levels (in ng/gDW) in control (blue), cold (red), and drought (green) conditions (mean ± SE with $n = 3$ replicates). (*F*) Measured leaf cross-sectional areas in control, cold, and drought conditions (mean ± SE with $n = 10$ for drought, and $n = 12$ for cold). (*G*) Mean GA concentrations (in nM) calculated using data in (*E*) and (*F*) and *SI Appendix*, Fig. S3. (*H*–*Q*) Metabolite and enzyme distributions in control (blue), cold (red), and drought (green) conditions. Data shown with stars and fitted model predictions with solid lines. (*D*, *E*, *G*, and *O*) show bars at the x-axis marking the mean DZ region for control (blue), drought (green), and cold (red) conditions ($n = 3$). Predictions in (*H*–*Q*) use the reduced model and assume that the activity of GA20ox is changed under drought conditions, whereas the activity of GA2ox is changed under cold conditions. Metabolite data (*H*, *L*–*Q*) show mean concentrations calculated from mean values from data on metabolite levels (*SI Appendix*, Fig. S4), dry weight (*SI Appendix*, Fig. S3*C*), and leaf cross-sectional area (*SI Appendix*, Fig. S3*A*). Transcript data (*I*–*K*) show mean values for $n = 3$–7 (positions 0–30 and 95 mm) and $n = 1$–3 (positions 35–85 mm).

conclude that the spatial variations in both GA_{53} and enzyme transcription are essential to create the GA_1 distribution that underpins growth regulation.

Activity of the heterologous GA20ox is higher than the native enzyme. We next set out to test whether the reduced model could explain the effect of experimental perturbations on GA metabolism, distribution, and leaf growth. We first studied the effects of overexpressing the AtGA20-oxidase1 biosynthesis enzyme (UBI::GA20-OX-1), which enhances bioactive GA levels and growth in both *Arabidopsis* (43, 44) and maize by increasing DZ size (9) (Fig. 4*A*). To investigate how overexpressing AtGA20-oxidase1 affects the metabolism dynamics, we simulated the UBI::GA20-OX-1 dynamics by including an additional enzyme, AtGA20ox, in the reduced model and incorporating terms representing the rate at which the AtGA20ox enzyme mediates the three oxidation steps: GA_{53} to GA_{44}, GA_{44} to GA_{19}, and GA_{19} to GA_{20}. Initially, we assumed that for each of these steps the native and heterologous *GA20ox* enzyme transcripts mediate the same rate of metabolite oxidation, and we

tried to fit the reduced model to metabolite and transcript data from wild-type and UBI::GA20-OX-1 (9). With this assumption, we found that the reduced model could not recapitulate the spatial distributions of transcript and metabolite levels observed experimentally (*SI Appendix*, Fig. S17); the reduced model suggests that for the downstream GAs to be higher in UBI::GA20-OX-1 requires GA_{53} to also be higher, which is not reflected in the experimental data (Fig. 4 *B* and *G*–*L*).

We solved this conundrum by allowing each of the three GA20ox-mediated oxidation rates to be different between the native and heterologous enzymes, which led to reasonable agreement between the reduced model and data (Fig. 4 *B*–*L*). Considering the estimated parameters (*SI Appendix*, Table S4), the estimated conversion rate of GA_{53} to GA_{44} is ∼20 times higher for AtGA20-oxidase1 and the conversion rates of GA_{44} to GA_{19} and GA_{19} to GA_{20} are approximately double that of the native enzyme. This explains why downstream GA concentrations were higher in the overexpression line (Fig. 4 *G*–*L*) despite GA_{53} concentrations being lower (Fig. 4*B*). These differences are likely due to differences in translation efficiency, protein degradation, or enzyme activity between the native and heterologous enzymes. The reduced model shows that the differences in GA20ox activity result in the GA_1 concentration having a higher maximum but decreasing to a similar level at the boundary between the DZ and EZ (at approximately 18 mm and 25 mm from the leaf base for wild-type and UBI::GA20-OX-1, respectively) (Fig. 4*J*), consistent with the GA_1 distribution controlling the DZ size via a threshold mechanism (i.e., the transition to the EZ occurring where GA_1 levels decrease below a threshold value) (9). We conclude that the reduced model recapitulates published data and identifies details in the molecular regulation of GA metabolism, such as differential specificity in the activities of the native and heterologous gene product.

Drought and cold regulate distinct enzymatic reactions. Next, we used the reduced model to determine whether and how GA distributions are affected by environmental stress and if this could explain the growth response. We applied the reduced model to published experimental data involving drought conditions (30) and newly collected data in cold conditions (31). Both stresses reduced the leaf elongation rate by 20 to 30% (30, 31) (Fig. 5 *A* and *B*), but this was due to different underlying cellular behaviors: a reduction in DZ size in drought conditions (30, 45) (Fig. 5*C* and *SI Appendix*, Table S3) and a reduction in division and elongation rates in cold conditions (31) (Fig. 5*D* and *SI Appendix*, Fig. S2).

Measured metabolite levels (in ng/gDW) showed GA_1 levels are reduced in both drought and cold conditions (Fig. 5*E*). We first converted these measurements to concentrations (nM), taking into account the cross-sectional area. In drought, cross-sectional areas are similar to those of the control (Fig. 5*F*), so that as for the GA_1 measurements, GA_1 concentrations (in nM) are also reduced (Fig. 5*G*). However, in cold, cross-sectional areas are much lower (Fig. 5*F*), resulting in GA_1 concentrations that are in fact similar to those in control conditions (Fig. 5*G*). We concluded that drought conditions, but not cold conditions, reduce the GA_1 concentrations. Measured GA_{53} levels (in ng/gDW) were little affected by drought or cold (*SI Appendix*, Fig. S4), resulting in GA_{53} concentrations that were increased in cold (once converted to nM), suggesting that cold affects the pathway upstream of GA_{53} (Fig. 5*H*). These observations illustrate the importance of conversion to nM concentrations when interpreting metabolite measurements.

Measurements of transcript levels revealed that drought reduces *GA20ox* levels and increases *GA2ox* levels (Fig. 5 *I* and *K*), whereas cold reduces *GA2ox* levels (Fig. 5*K*). We first tested whether these perturbed enzyme transcript levels cause the observed metabolite distributions, assuming identical oxidation rate constants, by fitting the reduced model to the control, cold and drought transcript and metabolite data. With this assumption, we were unable to reproduce the metabolite distributions (*SI Appendix*, Fig. S18). The predicted difference between GA_1 in control and drought conditions was much less than observed, whereas GA_1 was predicted to be higher in cold than in control conditions, again in contrast to the data.

To resolve this discrepancy, we hypothesized that drought and cold regulate the GA pathway by additional mechanisms (e.g., translation, protein stability, or enzyme activity). To test this theory, we fitted the reduced model to the data, allowing the oxidation rate constants for either the GA20ox-mediated steps, the GA3ox-mediated step, or the GA2ox-mediated steps to be different in cold and drought. To select among the resulting 16 possible cases (*SI Appendix*, Table S5), we used the Akaike Information Criterion (AICc) (46), a statistical measure that assesses the goodness of fit while penalizing model complexity by taking into account the number of model parameters. Fitting the model and calculating the AICc in each case provided a means to select among the possible cases. Considering the AICc values obtained (*SI Appendix*, Table S5), our results suggest that the rate constants governing the GA20ox-mediated steps are perturbed in drought and that the rate constants governing the GA2ox-mediated steps are perturbed in cold (Fig. 5 *H*–*Q*). The parameter estimates (*SI Appendix*, Table S6) suggest that in drought, the conversion rates of GA_{53} to GA_{44} and GA_{19} to GA_{20} are similar to those in control conditions, whereas the conversion rate of GA_{44} to GA_{19} is approximately doubled, providing an explanation as to why GA_{19} concentrations are similar in drought and control conditions while GA_{44} is lower in drought. The parameter estimates suggest that in cold the degradation rates of both GA_{20} and GA_{29} are higher than in control conditions, so that overall degradation is substantially increased in cold despite the *GA2ox* transcript levels being lower.

Thus, our modeling approach identifies specific GA enzyme activities impacted by drought and cold and explains the observed metabolite levels. Although in drought *GA20ox* transcript levels are lower than in control conditions (Fig. 5*I*), the reduced model predicts that GA20ox enzymes mediate the GA_{44}-to-GA_{19} oxidation step at a higher rate. This prediction suggests that GA_1 synthesis in drought is similar to that in control conditions and that the lower GA_1 concentrations are caused by increased degradation mediated by increased *GA2ox* transcript levels. In cold, the *GA2ox* transcripts are expressed at lower levels than in control conditions, but the rate constant associated with GA2ox-mediated GA_{20} degradation is increased, explaining why GA_1 concentrations are similar in control and cold conditions.

Enzyme activity measurements support model predictions. To test the surprising model prediction that enzyme activities (relative to their transcript levels) increase in response to cold and drought, we performed further experiments to measure the enzyme activity directly. We considered six reactions for each condition: GA_{53}, GA_{44}, and GA_{19} were used to determine GA20ox activities, and GA_1, GA_{29}, and GA_8 were used to obtain GA2ox activities. The enzymes were extracted from 10 mm segments from the maize leaf growth zone. These data

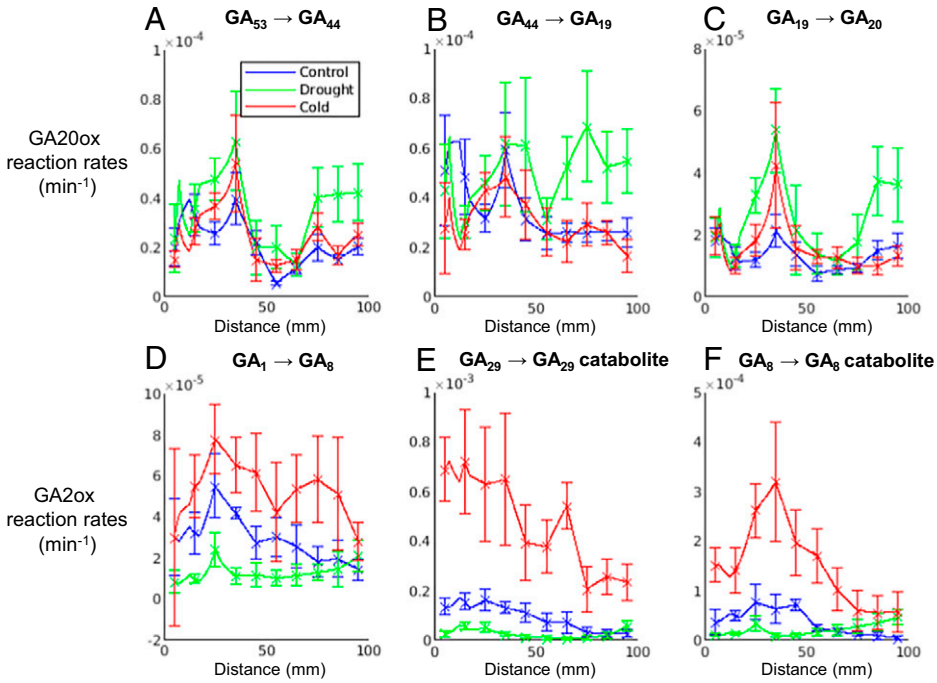

Fig. 6. Reaction rates calculated from measurements of enzyme activity for control (blue) drought (green), and cold (red) conditions. (*A–C*) Reactions mediated by GA20ox: GA_{53} to GA_{44} (*A*), GA_{44} to GA_{19} (*B*), and GA_{19} to GA_{20} (*C*). (*D–F*) Reactions mediated by GA2ox: GA_1 to GA_8 (*D*), GA_{29} to GA_{29} catabolite (*E*), and GA_8 to GA_8 catabolite (*F*). Data show mean ± SE calculated from degradation rate data (*SI Appendix*, Fig. S19, $n = 3$) and enzyme transcript levels (Fig. 5 *H–J*, $n = 1–7$).

(*SI Appendix*, Fig. S19) were used to calculate the oxidation rate constants (*SI Appendix* contains details).

In agreement with the model predictions, the oxidation rate mediated by GA2ox increased in cold conditions (Fig. 6). For drought, there was a trend for higher oxidation rates associated with GA20ox activity, also in support of the model predictions. Therefore, these in vivo activity measurements support the in silico prediction of increased specific enzyme activities in cold (GA2ox) and drought (GA20ox) conditions.

Discussion

GA regulates plant growth and growth response to environmental conditions (1, 2). Understanding how local bioactive GA levels are controlled is key to understanding these growth responses. However, often in studies of GA metabolism only static measurements are made of metabolite and transcript levels. Although static measurements have led to profound insight into how GA regulates growth, our approach to use computational modeling in combination with in vivo measurements allows us to expand our knowledge to the dynamics of the reactions in responses to heterologous transgenes and environmental conditions.

We presented a mathematical model that simulates the key cellular and subcellular processes governing GA distribution in the maize leaf growth zone. The modeling revealed that the bioactive GA_1 distribution is predominantly determined by the spatial variations in metabolism. We validated the model by demonstrating that it recapitulates experimental data from both wild-type and plants overexpressing the AtGA20-oxidase1 biosynthesis enzyme (UBI::GA20-OX-1). This revealed that the heterologous AtGA20-oxidase1 enzyme is substantially more active than the native maize version, with a much higher rate of conversion of GA_{53} to GA_{44}.

The model also allowed us to obtain drought and cold responses that could not be deduced from the gene expression and metabolite distributions alone. The modeling suggested that the GA_1 concentrations in the stressed conditions are not the result of changes in enzyme transcript levels alone. Instead, oxidation rates associated with specific enzymes were increased in the stressed conditions, suggesting that stress-induced post-transcriptional regulation of enzyme activities has a major effect on GA_1 levels under these conditions. Subsequent enzyme–activity assays validated these model predictions, suggesting that further studies of GA oxidation enzymes at the protein level are needed to understand the regulation of bioactive GA levels and growth.

The predicted GA_1 distributions provide an explanation for how GA metabolism regulates the growth dynamics. Higher GA_1 concentrations in UBI::GA20-OX-1 and the lower GA_1 concentrations under drought shift the position at which the GA_1 reaches a threshold value thought to determine the DZ length (9, 30) (i.e., a larger DZ in UBI::GA20-OX-1 and a smaller DZ in drought). The modeling enabled us to identify which specific oxidation steps are affected in these cases to create this GA_1 distribution and growth response. The reduction in leaf growth in cold is due to a different cellular mechanism: a reduction in division and elongation rates rather than DZ length (31). Our study revealed that once converted to nM concentrations, the GA_1 distribution in cold conditions is approximately the same as in control conditions, explaining why the growth zone lengths are not affected. Our findings therefore suggest that the growth inhibition by cold does not appear to be regulated by the GA pathway.

While the model predictions generally agreed well with the experimental measurements, there were naturally some differences. These differences may have been caused by variability in the data (for instance, differences between the predictions and data at the GA_1 peak in the control case in Fig. 5*O* may be caused by the relatively large SEs in the measured GA_1 levels in this region, shown in Fig. 5*E*). Additional differences may be caused by biological phenomena or variability not explicitly considered in the model.

Fitting the model to the data required us to develop a reduced model. Although cell-based models, which simulate populations of dividing and growing cells, are often used to investigate hormone dynamics (13, 29, 47), the simulation times involved typically make formal parameter estimation impractical. Simulations are particularly slow for the maize leaf growth zone, which contains ∼1,400 cells in each file (31), in contrast to only ∼70 in *Arabidopsis* (48). It was therefore necessary to derive a continuum approximation of the cell-based model. This approach, to move from the Lagrangian (or material) viewpoint to the Eulerian (or spatial) one, has played a major role in understanding plant growth kinematics (49–51), although it has received limited attention by hormone modelers (52, 53). We also considered methods for integrating spatially varying inputs (i.e., components that are regulated by upstream processes not included in the model) via b-spline representations. There is much potential to translate these modeling approaches to study dynamics in other cell-based systems.

Our study demonstrates the usefulness of a detailed model of GA metabolism within the growing maize leaf. To gain a more complete insight, this model could be extended, for example, to investigate the downstream GA signaling pathway and growth regulation, the parallel pathway that mediates the synthesis of the bioactive GA_4 (which is the main bioactive GA in other species such as *Arabidopsis* (54)), GA metabolism dynamics in other plant organs, or how GA metabolism enzymes are regulated by other hormones (29, 55). Furthermore, the transcript and metabolite measurements used here are from the entire leaf segment, although in *Arabidopsis* roots, GA levels and responses have been shown to vary between tissues (8, 56, 57). Studying whether differences between tissues exist in maize leaves could motivate a more detailed 2-dimensional or 3-dimensional model that incorporates cellular geometries and tissue-specific processes. Such model developments would be able to reveal further details regarding the intricate and interacting multiscale interactions involved in organ growth regulation.

Methods

Modeling. Full details of the mathematical model are provided in the *SI Appendix*. We defined a cell-based model integrating growth, metabolism, and dilution (*SI Appendix*, section 2) and used this to derive a reduced model (*SI Appendix*, section 3). We simulated the reduced model by specifying growth using experimental measurements (*SI Appendix*, section 2.3.1) and used the metabolite and transcript data to estimate the reduced model parameters using Matlab's lsqnonlin optimization algorithm (*SI Appendix*, section 2.3.2–4). All code and data are provided in a GitLab repository.

Plant material and growth conditions. Plant material and growth conditions were as described in ref. (31) (cold) and ref. (30) (drought).

Hormone profiling. For hormone profiling, sampling, extraction, purification, and hormone metabolic profiling were performed as described in ref. (9). Data for the UBI::GA20OX-1 experiment (Fig. 4, Fig S5) were reprinted from ref (9 Current Biology, Vol: 22, Hilde Nelissen, Bart Rymen, Yusuke Jikumaru, Kirin Demuynck, Mieke Van Lijsebettens, Yuji Kamiya, Dirk Inze, and Gerrit T.S. Beemster, A Local Maximum in Gibberellin Levels Regulates Maize Leaf Growth by Spatial Control of Cell Division, p1183-1187, 2012, with permission from Elsevier.

Transcript levels. Enzyme transcript levels were measured as described in ref. (9). Transcript data for the UBI::GA20OX-1 experiment (Fig. 4) are as published in ref. (9). In the drought–cold experiment (Fig. 5), *GA20ox* levels are the summation of the measured levels of *GA20ox1*, *GA20ox2.1*, and *GA20ox2.2*; *GA3ox* is the level of *GA3ox2*; and *GA2ox* levels are the summation of *GA2ox3.1*, *GA2ox3.2*, *GA2ox4*, *GA2ox6.2*, *GA2ox7.1*, and *GA2ox7.3*, each measurement being the mean of $n = 3$ to 7 replicates for positions 0 to 30, located around the GA maximum; 95 mm, located at the end of the growth zone; and of $n = 1$ to 3 replicates for positions 35 to 85 mm, where GA levels are relatively stable.

Kinematic analysis. Kinematic analysis and measurements of division–zone length were performed as described in ref. (32). The cross-sectional areas were calculated by measuring the volumes of 1 cm segments of leaf.

Assay of GA metabolism enzymes. Enzymes were extracted from 10 segments of the fourth maize leaf, and enzyme activities were measured directly as described in *SI Appendix*, section 1.

Data Availability. All code and data used in this paper have been deposited in GitLab (https://gitlab.com/leahband/ga_maize_project/).

ACKNOWLEDGMENTS. This work was supported by the Leverhulme Trust (Early Career Fellowship to Dr. Leah Band, ECF-2012-681) and the Human Frontier Science Program (grant number RGY0075/2020).

Author affiliations: [a]Division of Plant and Crop Sciences, School of Biosciences, University of Nottingham, Sutton Bonington LE12 5RD, United Kingdom; [b]School of Mathematical Sciences, University of Nottingham, Nottingham NG7 2RD, United Kingdom; [c]Department of Plant Biotechnology and Bioinformatics, Ghent University, 9052 Ghent, Belgium; [d]VIB Center for Plant Systems Biology, 9052 Ghent, Belgium; [e]KU Leuven Plant Institute (LPI), KU Leuven, Kasteelpark Arenberg 31, B-3001 Leuven, Belgium; [f]Integrated Molecular Plant Physiology Research, Department of Biology, University of Antwerp, 2020 Antwerp, Belgium; and [g]Department of Botany and Microbiology, Science Faculty, Beni-Suef University, Beni-Suef 62511, Egypt

1. E. H. Colebrook, S. G. Thomas, A. L. Phillips, P. Hedden, The role of gibberellin signalling in plant responses to abiotic stress. *J. Exp. Biol.* **217**, 67–75 (2014).
2. H. Claeys, S. De Bodt, D. Inzé, Gibberellins and DELLAs: Central nodes in growth regulatory networks. *Trends Plant Sci.* **19**, 231–239 (2014).
3. A. Gázquez, G. T. S. Beemster, What determines organ size differences between species? A meta-analysis of the cellular basis. *New Phytol.* **215**, 299–308 (2017).
4. J. T. Arredondo, S. Hans, Components of leaf elongation rate and their relationship to specific leaf area in contrasting grasses. *New Phytol.* **158**, 305–314 (2003).
5. F. Fiorani, G. T. Beemster, Quantitative analyses of cell division in plants. *Plant Mol. Biol.* **60**, 963–979 (2006).
6. J.-L. Durand, R. Schäufele, F. Gastal, Grass leaf elongation rate as a function of developmental stage and temperature: Morphological analysis and modelling. *Ann. Bot. (Lond.)* **83**, 577–588 (1999).
7. S. Ubeda-Tomás, G. T. S. Beemster, M. J. Bennett, Hormonal regulation of root growth: Integrating local activities into global behaviour. *Trends Plant Sci.* **17**, 326–331 (2012).
8. S. Ubeda-Tomás *et al.*, Gibberellin signaling in the endodermis controls Arabidopsis root meristem size. *Curr. Biol.* **19**, 1194–1199 (2009).
9. H. Nelissen *et al.*, A local maximum in gibberellin levels regulates maize leaf growth by spatial control of cell division. *Curr. Biol.* **22**, 1183–1187 (2012).
10. F. M. Hetherington, M. Kakkar, J. F. Topping, K. Lindsey, Gibberellin signaling mediates lateral root inhibition in response to K+-deprivation. *Plant Physiol.* **185**, 1198–1215 (2021).
11. P. Achard *et al.*, Gibberellin signaling controls cell proliferation rate in Arabidopsis. *Curr. Biol.* **19**, 1188–1193 (2009).
12. I. Blilou *et al.*, The PIN auxin efflux facilitator network controls growth and patterning in Arabidopsis roots. *Nature* **433**, 39–44 (2005).
13. V. A. Grieneisen, J. Xu, A. F. Marée, P. Hogeweg, B. Scheres, Auxin transport is sufficient to generate a maximum and gradient guiding root growth. *Nature* **449**, 1008–1013 (2007).
14. R. Di Mambro *et al.*, Auxin minimum triggers the developmental switch from cell division to cell differentiation in the *Arabidopsis* root. *Proc. Natl. Acad. Sci. U.S.A.* **114**, E7641–E7649 (2017).
15. R. Dello Ioio *et al.*, A genetic framework for the control of cell division and differentiation in the root meristem. *Science* **322**, 1380–1384 (2008).
16. E. Salvi *et al.*, A self-organized PLT/auxin/ARR-B network controls the dynamics of root zonation development in Arabidopsis thaliana. *Dev. Cell* **53**, 431–443.e23 (2020).
17. V. Avramova, K. Sprangers, G. T. S. Beemster, The maize leaf: another perspective on growth regulation. *Trends Plant Sci.* **20**, 787–797 (2015).
18. A. Rizza, A. Walia, V. Lanquar, W. B. Frommer, A. M. Jones, In vivo gibberellin gradients visualized in rapidly elongating tissues. *Nat. Plants* **3**, 803–813 (2017).
19. P. Achard *et al.*, The cold-inducible CBF1 factor-dependent signaling pathway modulates the accumulation of the growth-repressing DELLA proteins via its effect on gibberellin metabolism. *Plant Cell* **20**, 2117–2129 (2008).
20. Y. Yamauchi *et al.*, Activation of gibberellin biosynthesis and response pathways by low temperature during imbibition of Arabidopsis thaliana seeds. *Plant Cell* **16**, 367–378 (2004).
21. H. Magome, S. Yamaguchi, A. Hanada, Y. Kamiya, K. Oda, The DDF1 transcriptional activator upregulates expression of a gibberellin-deactivating gene, GA2ox7, under high-salinity stress in Arabidopsis. *Plant J.* **56**, 613–626 (2008).
22. C. Jiang, X. Gao, L. Liao, N. P. Harberd, X. Fu, Phosphate starvation root architecture and anthocyanin accumulation responses are modulated by the gibberellin-DELLA signaling pathway in Arabidopsis. *Plant Physiol.* **145**, 1460–1470 (2007).

23. T. Hisamatsu, R. W. King, C. A. Helliwell, M. Koshioka, The involvement of gibberellin 20-oxidase genes in phytochrome-regulated petiole elongation of Arabidopsis. *Plant Physiol.* **138**, 1106–1116 (2005).
24. M. Dubois *et al.*, Ethylene response factor6 acts as a central regulator of leaf growth under water-limiting conditions in Arabidopsis. *Plant Physiol.* **162**, 319–332 (2013).
25. D. Weiss, N. Ori, Mechanisms of cross talk between gibberellin and other hormones. *Plant Physiol.* **144**, 1240–1246 (2007).
26. M. Frigerio *et al.*, Transcriptional regulation of gibberellin metabolism genes by auxin signaling in Arabidopsis. *Plant Physiol.* **142**, 553–563 (2006).
27. D. De Vos, K. Vissenberg, J. Broeckhove, G. T. Beemster, Putting theory to the test: Which regulatory mechanisms can drive realistic growth of a root? *PLOS Comput. Biol.* **10**, e1003910 (2014).
28. L. R. Band *et al.*, Growth-induced hormone dilution can explain the dynamics of plant root cell elongation. *Proc. Natl. Acad. Sci. U.S.A.* **109**, 7577–7582 (2012).
29. D. De Vos *et al.*, How grass keeps growing: An integrated analysis of hormonal crosstalk in the maize leaf growth zone. *New Phytol.* **225**, 2513–2525 (2020).
30. H. Nelissen *et al.*, The reduction in maize leaf growth under mild drought affects the transition between cell division and cell expansion and cannot be restored by elevated gibberellic acid levels. *Plant Biotechnol. J.* **16**, 615–627 (2018).
31. B. Rymen *et al.*, Cold nights impair leaf growth and cell cycle progression in maize through transcriptional changes of cell cycle genes. *Plant Physiol.* **143**, 1429–1438 (2007).
32. H. Nelissen *et al.*, Kinematic analysis of cell division in leaves of mono- and dicotyledonous species: A basis for understanding growth and developing refined molecular sampling strategies. *Methods Mol. Biol.* **959**, 247–264 (2013).
33. K. Sprangers, S. Thys, D. van Dusschoten, G. T. S. Beemster, Gibberellin enhances the anisotropy of cell expansion in the growth zone of the maize leaf. *Front Plant Sci* **11**, 1163 (2020).
34. N. A. Jolliffe, C. P. Craddock, L. Frigerio, Pathways for protein transport to seed storage vacuoles. *Biochem. Soc. Trans.* **33**, 1016–1018 (2005).
35. S. Yamaguchi, Gibberellin metabolism and its regulation. *Annu. Rev. Plant Biol.* **59**, 225–251 (2008).
36. P. Hedden, S. G. Thomas, Gibberellin biosynthesis and its regulation. *Biochem. J.* **444**, 11–25 (2012).
37. C. M. Fleet *et al.*, Overexpression of AtCPS and AtKS in Arabidopsis confers increased ent-kaurene production but no increase in bioactive gibberellins. *Plant Physiol.* **132**, 830–839 (2003).
38. A. M. Middleton *et al.*, Mathematical modeling elucidates the role of transcriptional feedback in gibberellin signaling. *Proc. Natl. Acad. Sci. U.S.A.* **109**, 7571–7576 (2012).
39. E. Shani *et al.*, Gibberellins accumulate in the elongating endodermal cells of Arabidopsis root. *Proc. Natl. Acad. Sci. U.S.A.* **110**, 4834–4839 (2013).
40. J. O. Ramsay, B. W. Silverman, *Functional Data Analysis* (Springer, ed. 2, 2005).
41. J. D. Murray, *Mathematical Biology I. An Introduction* (Springer, ed. 3, 2002).
42. L. R. Band, S. P. Preston, Parameter inference to motivate asymptotic model reduction: An analysis of the gibberellin biosynthesis pathway. *J. Theor. Biol.* **457**, 66–78 (2018).
43. J. P. Coles *et al.*, Modification of gibberellin production and plant development in Arabidopsis by sense and antisense expression of gibberellin 20-oxidase genes. *Plant J.* **17**, 547–556 (1999).
44. N. Gonzalez *et al.*, Increased leaf size: Different means to an end. *Plant Physiol.* **153**, 1261–1279 (2010).
45. V. Avramova *et al.*, Drought induces distinct growth response, protection, and recovery mechanisms in the maize leaf growth zone. *Plant Physiol.* **169**, 1382–1396 (2015).
46. K. P. Burnham, D. R. Anderson, *Model Selection and Multimodel Inference: A Practical Information-Theoretic Approach* (Springer-Verlag, New York, NY, ed. 2, 2002).
47. H. Jönsson, M. G. Heisler, B. E. Shapiro, E. M. Meyerowitz, E. Mjolsness, An auxin-driven polarized transport model for phyllotaxis. *Proc. Natl. Acad. Sci. U.S.A.* **103**, 1633–1638 (2006).
48. G. T. S. Beemster, T. I. Baskin, Analysis of cell division and elongation underlying the developmental acceleration of root growth in Arabidopsis thaliana. *Plant Physiol.* **116**, 1515–1526 (1998).
49. W. K. Silk, R. O. Erickson, Kinematics of plant growth. *J. Theor. Biol.* **76**, 481–501 (1979).
50. W. K. Silk, Quantitative descriptions of development. *Annu. Rev. Plant Physiol.* **35**, 479–518 (1984).
51. W. K. Silk, M.-B. Bogeat-Triboulot, Deposition rates in growing tissue: Implications for physiology, molecular biology, and response to environmental variation. *Plant Soil* **374**, 1–17 (2013).
52. G. J. Mitchison, The dynamics of auxin transport. *Proc. R. Soc. Lond. B Biol. Sci.* **209**, 489–511 (1980).
53. L. R. Band, J. R. King, Multiscale modelling of auxin transport in the plant-root elongation zone. *J. Math. Biol.* **65**, 743–785 (2012).
54. S. Eriksson, H. Böhlenius, T. Moritz, O. Nilsson, GA4 is the active gibberellin in the regulation of LEAFY transcription and Arabidopsis floral initiation. *Plant Cell* **18**, 2172–2181 (2006).
55. H. R. Allen, M. Ptashnyk, Mathematical modelling and analysis of the brassinosteroid and gibberellin signalling pathways and their interactions. *J. Theor. Biol.* **432**, 109–131 (2017).
56. S. Ubeda-Tomás *et al.*, Root growth in Arabidopsis requires gibberellin/DELLA signalling in the endodermis. *Nat. Cell Biol.* **10**, 625–628 (2008).
57. I. Tal *et al.*, The arabidopsis NPF3 protein is a GA transporter. *Nat. Commun.* **7**, 11486 (2016).